Real-Time Reference Position Shaping to Reduce Vibration in Slewing of a Very-Flexible-Joint Robot

Withit Chatlatanagulchai[1], Kanokrat Saeheng[2]
Control of Robot and Vibration Laboratory (CRV Lab),
Department of Mechanical Engineering, Faculty of Engineering,
Kasetsart University, Bangkok, Thailand
E-mail: [1]fengwtc@ku.ac.th, [2]focous_ly@hotmail.com

Abstract

A very-flexible-joint robot is a manipulator in which a soft spring is placed at its joint to reduce damage in case of collision. Despite this benefit, slewing of this robot is less accurate because of the link vibration. The convolution between the reference position and a properly designed impulse sequence produces an input that cancels residual vibration resulting in smoother robot motion. The convolution can be done in real time; the technique is then suitable for human-operated machine such as construction crane and tele-operated boom. In this paper, we apply this technique to a laboratory-scale human-operated very-flexible-joint robot with excellent vibration-attenuated results.

Key Words: Vibration Reduction, Flexible Joint, Input Shaping, Shaped Reference Inputs, Convolution

Introduction

It would be nice to be able to put springs in the joints of the manipulators so that when they accidentally hit something, the damage can be greatly reduced due to the joint flexibility. However, joint flexibility does exist in all robot manipulators. The joint is flexible as a result of the elastic property of its material, such as those of driving actuator, gear teeth, or transmission belt.

Even the smallest amount of flexibility can be excited resulting in severe oscillations if not properly accounted for in the control design phase, as pointed out by Sweet and Good (1984.) In the past, researchers have dealt with this joint flexibility using either active control, where external energy is provided to the system to attenuate oscillations, or passive control, where no external energy is provided, but instead the structure of the system is altered, mostly to damp out the oscillations, or the reference inputs are shaped to avoid exciting the closed-loop system.

In active control, Spong (1987) and Ge (1996) applied a singular perturbation method to the flexible-joint robot, where a slow control drives the closed-loop system to a quasi-steady-state rigid-joint system, then a fast control can be designed for the resulting rigid-joint system. Spong and Vidyasagar (1989) and De Luca and Lucibello (1998) applied static and dynamic feedback linearizations to the robot, but their methods require a vital assumption regarding the system kinetic energy. More nonlinear control such as passivity-based and backstepping controls can be found in the work of Brogliato et al. (1995.) A more-recent active control for the flexible-joint robot moves toward using intelligent systems such as the radial basis function network (Ge et al., 1998) and the fuzzy system (Park, 2004.)

While active controls have proliferated, passive controls, especially those that use reference input shaping, are less well-known. Meckl and Seering (1988) reconstructed a bang-bang reference acceleration signal using ramped sine or versine basis functions. A cost function is penalized, weighing over removing the spectrum energy around the natural frequencies and approaching the bang-bang shape. Chatlatanagulchai et al. (2006) applied this method with a two-link flexible-joint robot.

Another shaping method was devised by Singer and Seering (1990.) Instead of shaping the reference acceleration, their method shapes the reference position directly by convoluting it with a properly designed impulse sequence. In theory, this impulse sequence is designed such that all impulse responses cancel each other producing vibration-free movement. Since the convolution with an impulse can be conveniently performed in real time, this method has received more attention than the former method, even though its appearance is still rare.

This paper contains our experience in applying the Singer and Seering' shaping method to our human-operated very-flexible-joint robot. This laboratory-scale robot is made to follow any arbitrary angular position commanded by the operator. It can be viewed as a model of a construction crane only with a flexible joint. A simple PID controller is used in the closed-loop system. The result is that the robot can move with significantly less vibration when the shaped reference position is applied instead of an unshaped square-wave reference position.

The paper is organized as follows. In Section 2, we provide some basics of the input shaping method, some of which were originally omitted in the original work by Singer and Seering (1990.) Section 3 contains details of the robot in the experiment including determination of its natural frequency and damping ratio. Input shaping for this robot is also discussed here. Section 4 presents the experimental set-up and results. Conclusions are given in Section 5.

Input Shaping Basics

[1] Impulse Responses Cancellation

For a one-degree-of-freedom unforced linear system with damping, the response to an impulse with magnitude $\hat{F}_1$ is given by

$$y(t) = \frac{\hat{F}_1 e^{-\zeta\omega_n(t-t_1)}}{m\omega_n\sqrt{1-\zeta^2}} \sin\sqrt{1-\zeta^2}\,\omega_n(t-t_1),$$

where y is the response, ζ is damping ratio, ω_n is natural frequency, m is mass, and t_1 is the time the impulse applies. The response $y(t)$ above can be plotted as a solid line in Figure 1(a). Suppose there is another impulse $\hat{F}_2$ applied at time t_2. If its magnitude and timing are designed properly, its response (the dash line in Figure 1(a)) would cancel with that of the first impulse producing a vibration-free response (Figure 1(b).)

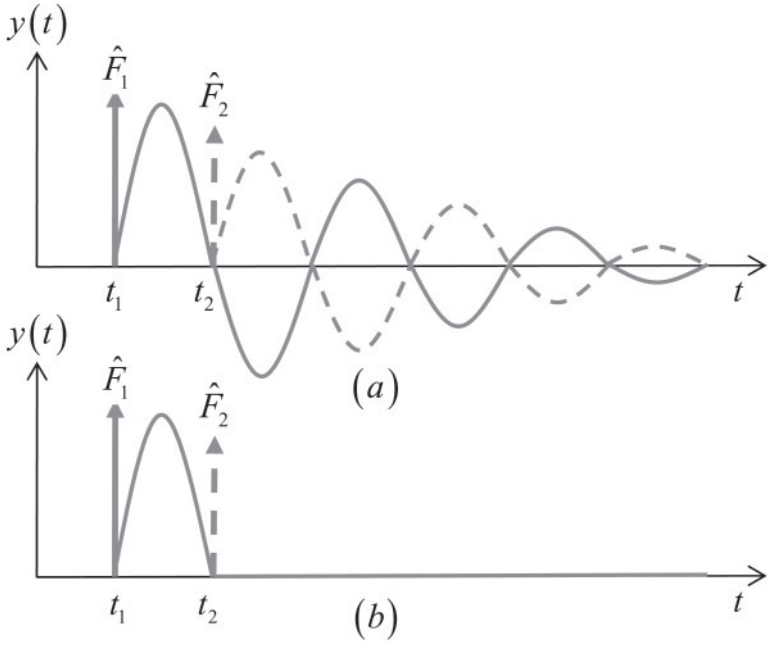

Figure 1 : System response of two impulses.

Suppose there are N impulses. Using the fact that

$$A_1 \sin(\alpha t + \beta_1) + A_2 \sin(\alpha t + \beta_2) = A \sin(\alpha t + \psi),$$

where

$$A = \sqrt{(A_1 \cos\beta_1 + A_2 \cos\beta_2)^2 + (A_1 \sin\beta_1 + A_2 \sin\beta_2)^2}$$

and

$$\psi = \tan^{-1}\left(\frac{A_1 \cos\beta_1 + A_2 \cos\beta_2}{A_1 \sin\beta_1 + A_2 \sin\beta_2}\right),$$

the sum of N impulse responses would result in an amplitude of

$$A = \sqrt{\left(\sum_{i=1}^{N} A_i \cos\beta_i\right)^2 + \left(\sum_{i=1}^{N} A_i \sin\beta_i\right)^2} \qquad (1)$$

with

$$A_i = \frac{\hat{F}_i e^{-\zeta\omega_n(t-t_i)}}{m\omega_n\sqrt{1-\zeta^2}} \qquad (2)$$

and

$$\beta_i = \sqrt{1-\zeta^2}\,\omega_n t_i.$$

Since we want to have zero-amplitude response right after the N^{th} impulse is applied, we set A in (1) to zero and t in (2) to t_N to have

$$\sum_{i=1}^{N} \frac{\hat{F}_i e^{-\zeta\omega_n(t_N - t_i)}}{m\omega_n\sqrt{1-\zeta^2}} \cos\sqrt{1-\zeta^2}\,\omega_n t_i = 0$$

and

$$\sum_{i=1}^{N} \frac{\hat{F}_i e^{-\zeta\omega_n(t_N - t_i)}}{m\omega_n\sqrt{1-\zeta^2}} \sin\sqrt{1-\zeta^2}\,\omega_n t_i = 0.$$

By multiplying both sides by $m\omega_n\sqrt{1-\zeta^2}$, the two equations above can be simplified to

$$\sum_{i=1}^{N} \hat{F}_i e^{-\zeta\omega_n(t_N - t_i)} \cos\sqrt{1-\zeta^2}\,\omega_n t_i = 0 \tag{3}$$

and

$$\sum_{i=1}^{N} \hat{F}_i e^{-\zeta\omega_n(t_N - t_i)} \sin\sqrt{1-\zeta^2}\,\omega_n t_i = 0. \tag{4}$$

For two impulses, of which the first one applies at $t_1 = 0$ and its impulse magnitude normalizes to $\hat{F}_1 = 1$, equations (3) and (4) have two unknowns t_2 and $\hat{F}_2$ and become

$$\hat{F}_2 \sin\left(t_2\omega_n\sqrt{1-\zeta^2}\right) = 0 \tag{5}$$

and

$$e^{-\zeta\omega_n(t_2)} + \hat{F}_2 \cos\left(t_2\omega_n\sqrt{1-\zeta^2}\right) = 0, \tag{6}$$

which can be readily solved to obtain

$$\hat{F}_2 = e^{-\frac{\zeta\pi}{\sqrt{1-\zeta^2}}} \text{ and } t_2 = \frac{\pi}{\omega_n\sqrt{1-\zeta^2}}.$$

2. *Robustness to Uncertainties in Natural Frequency and Damping Ratio*

The amount of residual vibration left depends on the accuracy of the natural frequency ω_n and the damping ratio ζ used to compute $\hat{F}_2$ and t_2. To increase the robustness of the input under variations of the natural frequency, we can set the derivatives, with respect to ω_n, of (3) and (4) to zeros to obtain two more constraints

$$\sum_{i=1}^{N} \hat{F}_i t_i e^{-\zeta\omega_n(t_N - t_i)} \cos\left(\sqrt{1-\zeta^2}\,\omega_n t_i\right) = 0 \tag{7}$$

and

$$\sum_{i=1}^{N} \hat{F}_i t_i e^{-\zeta\omega_n(t_N - t_i)} \sin\left(\sqrt{1-\zeta^2}\,\omega_n t_i\right) = 0. \tag{8}$$

The constraints (7) and (8) reduce the sensitivity of the constraints (3) and (4) to change in ω_n and can be used to solve for two additional unknowns t_3 and $\hat{F}_3$ of the third impulse.

Again, letting $t_1 = 0$ and $\hat{F}_1 = 1$, we can compute $t_2, \hat{F}_2, t_3,$ and $\hat{F}_3$ from (5)-(8) to be

$$t_2 = \frac{\pi}{\omega_n\sqrt{1-\zeta^2}},\ \hat{F}_2 = 2e^{\frac{-\zeta\pi}{\sqrt{1-\zeta^2}}},\ t_3 = \frac{2\pi}{\omega_n\sqrt{1-\zeta^2}},\ \text{and}\ \hat{F}_3 = e^{\frac{-2\zeta\pi}{\sqrt{1-\zeta^2}}}. \tag{9}$$

Increasing the robustness of the input under variations of the damping ratio requires setting derivatives of (3) and (4) with respect to ζ to zeros. It turns out that this produces the same constraints as (7) and (8).

To obtain even more robustness, we can continue to differentiate (7) and (8) to produce a new set of constraints for the fourth impulse and so on. However, doing so could result in slower trajectory when implementing in the closed-loop system as will be seen in the following section. Therefore, normally three impulses suffice for most applications.

3. Closed-Loop Application

The impulse sequence developed previously can be applied to the closed-loop system as an input shaper in Figure 2. The impulse sequence can be convolved with the reference position r to create a shaped input that will cancel the residual vibrations. Normally, if the controller G does not add any underdamped poles to the closed-loop system, the natural frequency and damping ratio still follow those of the plant P. If this is not the case, the impulse sequence must be designed with the closed-loop natural frequency and damping ratio.

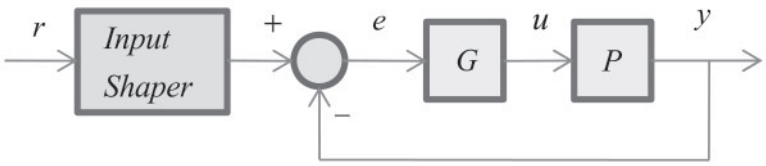

Figure 2 : Closed-loop-system block diagram with an input shaper.

As a time-domain operation, the convolution of two signals $f(t)$ and $g(t)$ is given by

$$f * g = \int_{-\infty}^{\infty} f(\tau) g(t-\tau)\, d\tau.$$

Since $g(t-\tau) = g(-\tau+t)$ can be viewed as a mirror image of $g(\tau)$ about the vertical axis shifting by the amount of t, the convolution result can be obtained graphically as Figure 3. Figure 3 (a) shows two example functions $f(\tau)$ and $g(\tau)$. Figure 3 (b) plots the mirror image $g(-\tau)$. Figure 3 (c) is when $g(-\tau)$ is shifted by t. Finally, Figure 3 (d) shows the resulting convolution $f * g$, which is the area under the product of $f(\tau)$ and $g(-\tau+t)$.

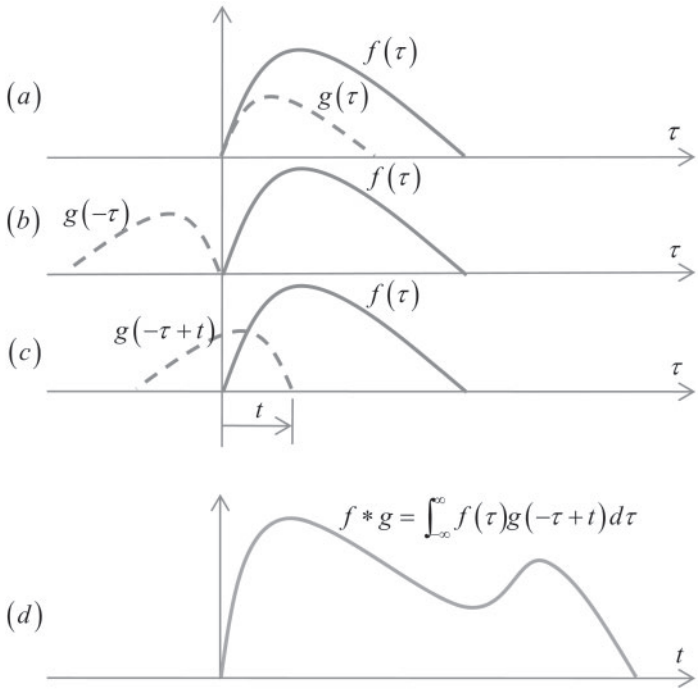

Figure 3 : Graphical interpretation of the convolution process.

For tracking, we need all impulse amplitudes to sum to one so that the shaped reference position will have the same end point as the original reference position. Therefore, in the three impulses case, the amplitudes and timing given in (9) can be plotted as Figure 4 (a), where

$$K = e^{-\frac{\zeta\pi}{\sqrt{1-\zeta^2}}}.$$

Figure 4 (b) shows the shaped step reference position, which is a result of convolving a step reference position r with the three-impulse sequence. This also shows that even though using more impulses provides more robustness, the shaped reference position will reach the end point at a later time t_N, where N is the number of impulses used.

Input Shaping of a Very-Flexible-Joint Robot

A diagram of a one-link flexible-joint robot is given in Figure 5. The motor rotates the block that connects to the link via two springs. Let θ_1 be the link angular position to be controlled, θ_2 be the motor or block angular position, $\ddot{x}$ be the tip linear acceleration, and v be the input voltage to the motor amplifier.

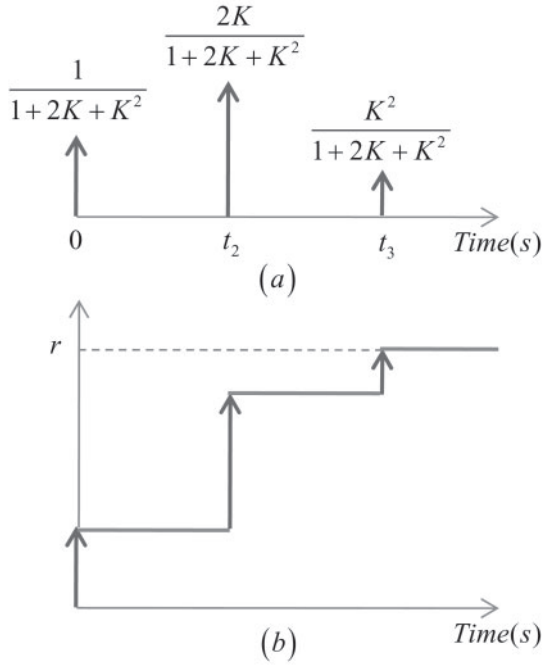

Figure 4 : (a) Three impulses. (b) Convolution of the impulse sequence with a step reference position *r*.

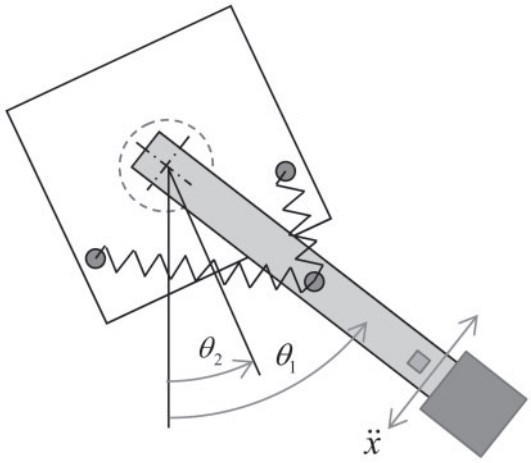

Figure 5 : Diagram of a one-link flexible-joint robot.

We can see that the motor controls the motor position θ_2, and the position θ_2 then affects the link position θ_1 though the spring. To obtain the damping ratio of the robot, we consider only the flexible portion. The transfer function from θ_2 to θ_1 is obtained from closed-loop system identifications using a simple PID controller and thirty-two frequency-varying sine waves as input voltages to the closed-loop system. We have

$$P_1 = \frac{\theta_1}{\theta_2} = \frac{c_1 s + c_0}{s^2 + d_1 s + d_0},$$

where $c_1 = [20.26, 22.39]$, $c_0 = [246.63, 272.59]$, $d_1 = [4.64, 5.13]$, $d_0 = [258.73, 285.96]$ are the uncertain ranges of parameters. Using the nominal values to obtain the damping ratio $\zeta = 0.15$.

For the natural frequency of the system, we record tip acceleration signal $\ddot{x}$ when the input voltages are several square waves with varying frequencies. The power spectrum of $\ddot{x}$ in Figure 6 reveals the natural frequency of $\omega_n = 10\, rad/s$. Note the uncertainty around the $10\, rad/s$, which will be handled by using three impulses instead of two.

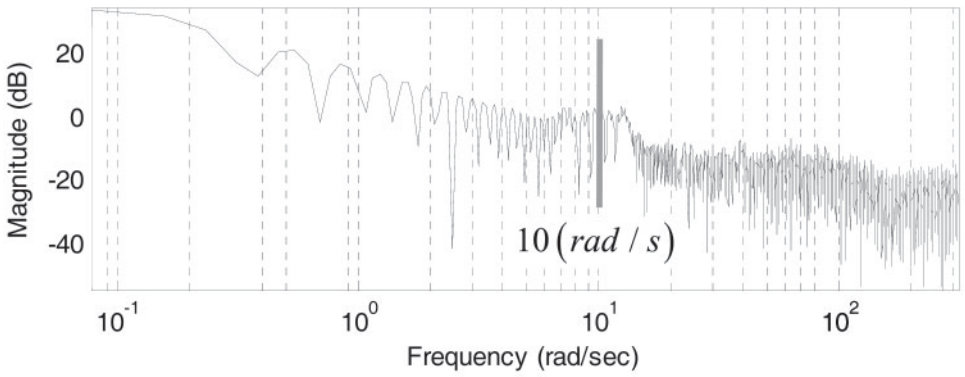

Figure 6 : Power spectrum of the tip acceleration signal having requency varying square wave as input voltage to the motor amplifier. The vertical line marks the system natural frequency.

Experimental Set-Up and Results

Figure 7 is a photograph of our flexible-joint robot. An accelerometer is mounted next to the payload located at the tip. The payload is varying due to the jiggling movement of some coins inside. Two optical encoders are used to measure the motor angle θ_2 and the link angle relative to the block $\theta_1 - \theta_2$. Both signals are added to produce the link absolute position θ_1 to be controlled. Two soft springs are attached to the link and the block to provide flexibility.

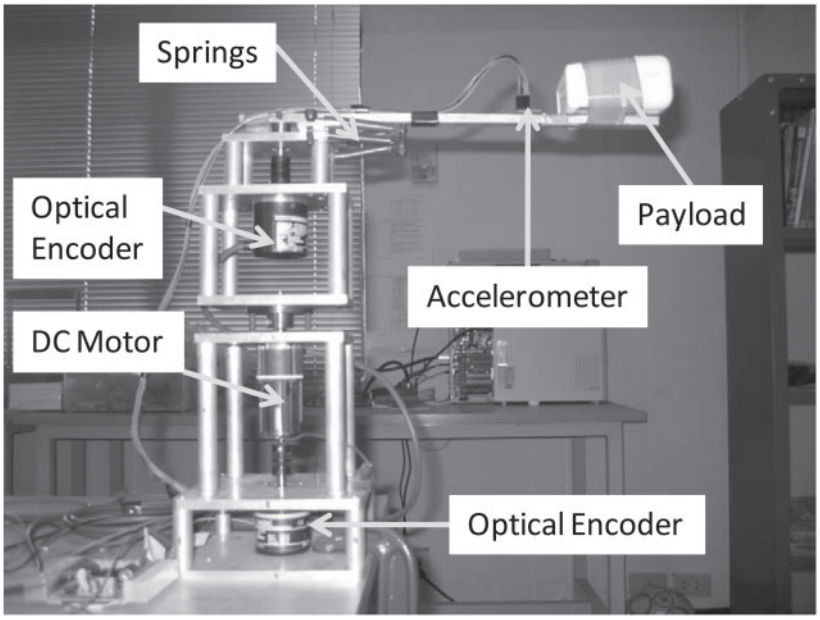

Figure 7 : Photograph of the flexible-joint robot in our laboratory.

Figure 8 is a block diagram of the experimental arrangement. A host computer, with necessary software, is used to communicate with the user and a target computer. The target computer contains a data acquisition card whose functions are to acquire sensor signals and to send out actuator commands from the control algorithm. The host and target computers are connected to each other via a LAN line. Control signal is sent as voltage to a motor amplifier board to amplify to a level that can drive the DC motor. An IC chip accelerometer is mounted at the tip to measure linear acceleration. A DC power supply supplies required current to the motor amplifier board.

A sampling time of $10\,ms$ is used for the hardware. The closed-loop controller is a simple PI controller with $K_p = 0.15$ and $K_I = 0.1$. This controller does not change the natural frequency and the damping ratio of the closed-loop system from those of the plant. Therefore, $\omega_n = 10\,rad/s$ and $\zeta = 0.15$ are used to design a sequence of three impulses using the formulas in (9).

A toggle switch is written in the program to turn the input shaper on and off. A turnable knob is also added to the program to let an operator control the robot as desired. The readings from the knob are interpreted as the reference position to be followed by the robot link absolute position θ_1.

Figure 9 plots the robot's link angular position θ_1 versus its desired trajectory θ_{1d} given arbitrarily by the operator. By alternating between the shaped and unshaped reference inputs, we clearly see that, with shaped input, the robot was able to settle faster with significantly less vibration than with the unshaped input, which suffers from severe residual vibration.

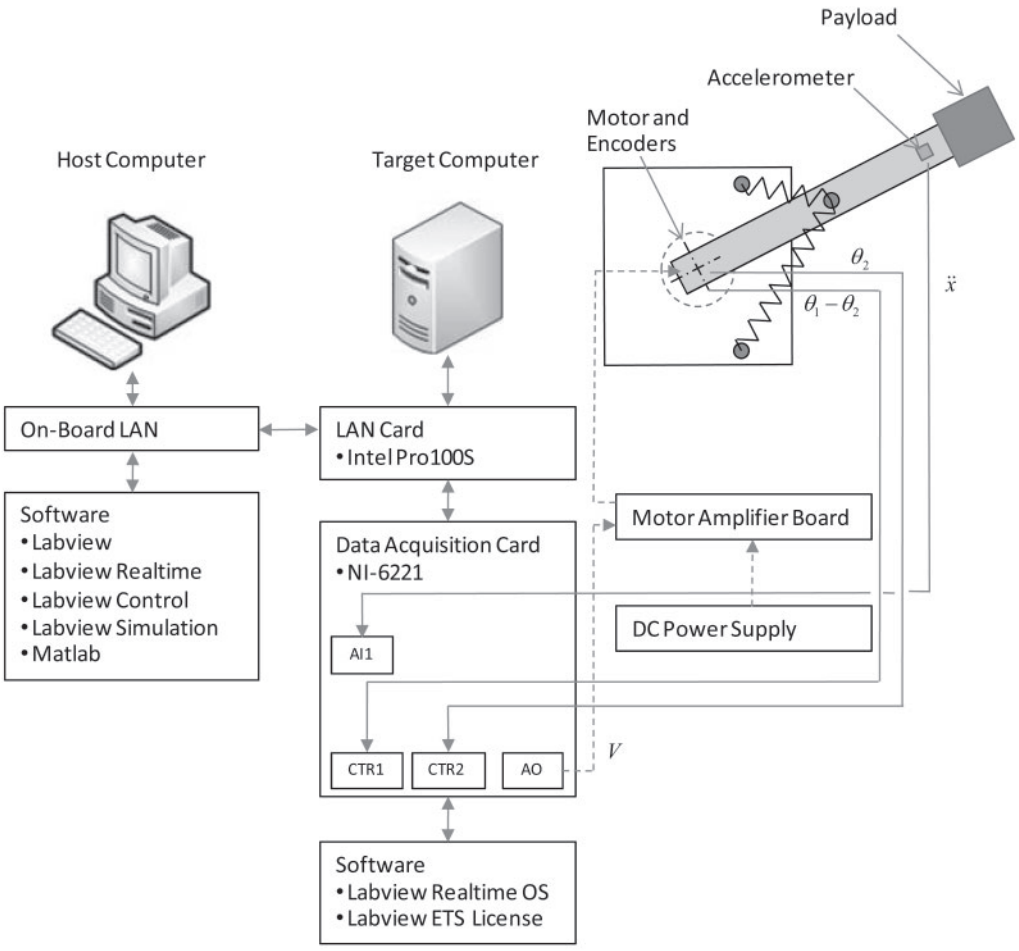

Figure 8 : Block diagram of the experimental set-up and associated hardware.

Figure 10 shows the signal from the accelerometer at the tip, with significantly higher acceleration output seen during the unshaped periods. The root-mean-square value of the acceleration is found to be 10 times higher during the unshaped period than during the shaped period. Figure 11 shows the control input voltage to the motor amplifier. The control input exhibits more chattering with higher amplitude during the unshaped period.

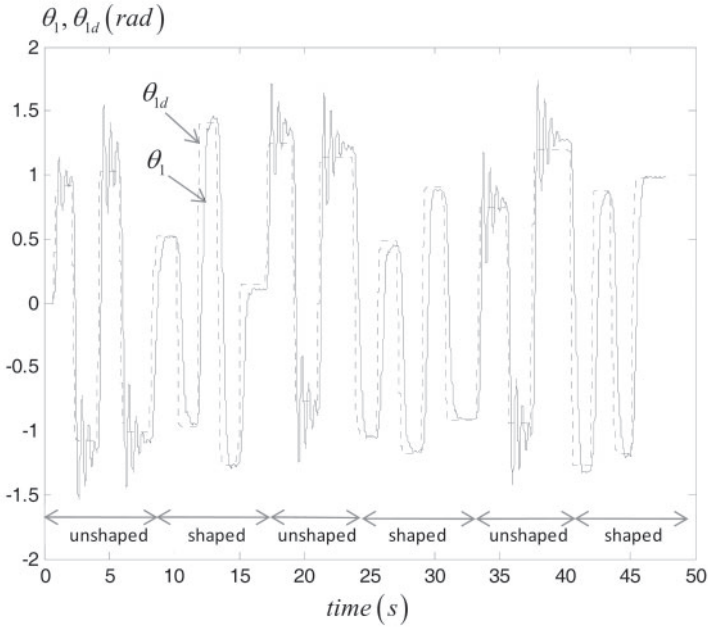

Figure 9 : Tracking result for shaped and unshaped cases: angular position output θ_1 (solid line) and its desired value θ_{1d} (dash line).

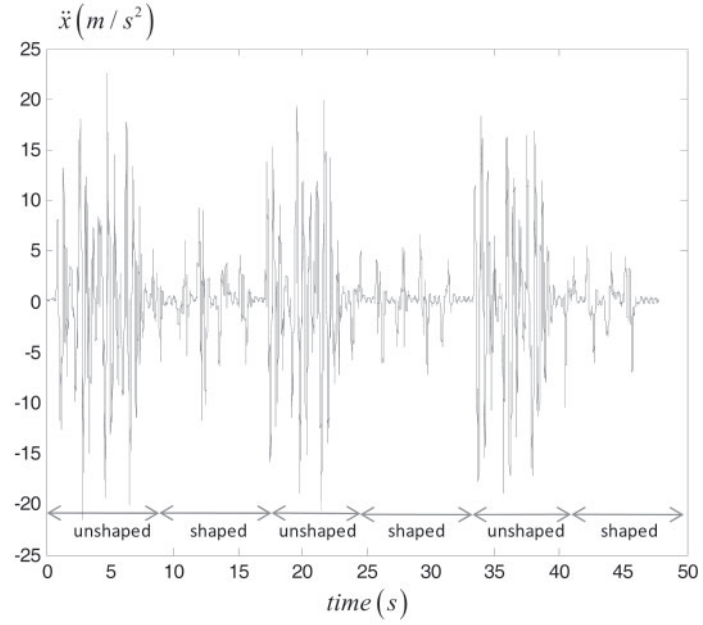

Figure 10 : Tip acceleration for shaped and unshaped cases.

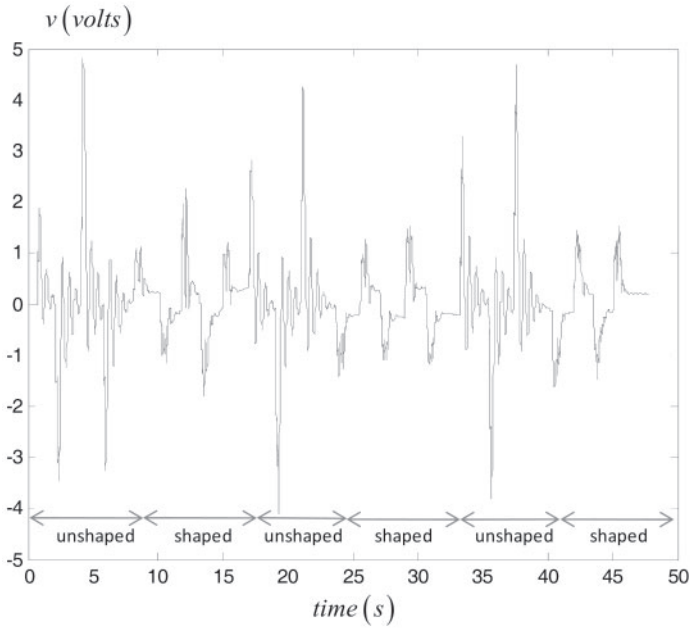

Figure 11 : Control input to the motor amplifier for shaped and unshaped cases.

Conclusions

Excellent vibration attenuation result was obtained with the flexible-joint robot having soft springs at its joint. The arbitrary reference position was convolved with a sequence of three impulses in real time producing a shaped input that cancels residual vibration of the system.

The potential application of this technique is extensive. It can be applied to human-operated construction cranes, gantry cranes, booms, robot manipulators, or any systems suffering from vibrations during slewing.

Nevertheless, the technique relies on the superposition principle of the linear system and, therefore, has no generalization to nonlinear systems. Further, the accuracy of the system's natural frequency and damping ratio is vital to the effectiveness of the technique. More research should be devoted to new robustness schemes or to adaptive or online parameter identification.

Acknowledgements

This work was performed at the Control of Robot and Vibration Laboratory, which is situated at and partially supported by the Research and Development Institute of Production Technology (RDiPT) of Kasetsart University, Thailand.

References

[1] Brogliato, B., R. Ortega, and R. Lozano. 1995. Global Tracking Controllers for Flexible-Joint Manipulators: a Comparative Study. Automatica. Vol. 31. No. 7. pp. 941-956.

[2] Chatlatanagulchai, W., V.M. Beazel, and P.H. Meckl. 2006. Command shaping applied to a flexible robot with configuration-dependent resonance. Proc. of the 2006 American Control Conference. Minneapolis. MN.

[3] De Luca, A. and P. Lucibello. 1998. A General Algorithm for Dynamic Feedback Linearization of Robots with Elastic Joints. Proceedings of the IEEE International Conference on Robotics and Automation. Belgium. pp. 504-510.

[4] Ge, S.S. 1996. Adaptive Control Design for Flexible Joint Manipulators. Automatica. Vol. 32. No. 2. pp. 273-278.

[5] Ge, S.S., T.H. Lee, and C.J. Harris. 1998. Adaptive Neural Network Control of Robotic Manipulators. World Scientific Publishing. Singapore.

[6] Meckl, P.H. and W.P. Seering. 1988. Controlling Velocity-Limited Systems to Reduce Residual Vibration. Proceedings of the 1998 IEEE International Conference on Robotics and Automation. Philadelphia. Pennsilvania.

[7] Park, C.W. 2004, Robust Stable Fuzzy Control via Fuzzy Modeling and Feedback Linearization with Its Applications to Controlling Uncertain Single-Link Flexible Joint Manipulators. Journal of Intelligent and Robotic Systems. Vol. 39. pp. 131-147.

[8] Singer, N.C. and W.P. Seering. 1990. Preshaping command inputs to reduce system vibration. ASME Trans. J. Dynam., Meas., Contr. Vol. 112. No. 1. pp. 76-82.

[9] Spong, M.W. 1987. Modeling and Control of Elastic Joint Robots. Transactions of the ASMEJournal of Dynamic Systems, Measurement and Control. Vol. 109. No. 4. pp. 310-319.

[10] Spong, M.W. and M. Vidyasagar. 1989. Robot Dynamics and Control. Wiley. New York.
[11] Sweet, L.M. and M.C. Good. 1984. Re-definition of the Robot Motion Control Problem: Effects of Plant Dynamics Drive System Constraints, and User Requirements. Proceedings of the 23rd IEEE Conference on Decision and Control. Las Vegas. NV. pp. 724-731.